SCIENTIFIC REPORTS

OPEN

SUBJECT AREAS:
COMPOSITES
CHEMICAL ENGINEERING

Received
28 May 2014

Accepted
16 July 2014

Published
4 August 2014

Correspondence and requests for materials should be addressed to C.J.L. (ughg_cjl@yahoo.com)

Three-dimensional Printed Acrylonitrile Butadiene Styrene Framework Coated with Cu-BTC Metal-organic Frameworks for the Removal of Methylene Blue

Zongyuan Wang, Jiajun Wang, Minyue Li, Kaihang Sun & Chang-jun Liu

Collaborative Innovation Center of Chemical Science and Engineering, School of Chemical Engineering and Technology, Tianjin University, Tianjin 300072, China.

Three-dimensional (3D) printing was applied for the fabrication of acrylonitrile butadiene styrene (ABS) framework. Functionalization of the ABS framework was then performed by coating of porous Cu-BTC (BTC = benzene tricarboxylic acid) metal-organic frameworks on it using a step-by-step *in-situ* growth. The size of the Cu-BTC particles on ABS was ranged from 200 nm to 900 nm. The Cu-BTC/ABS framework can take up most of the space of the tubular reactor that makes the adsorption effective with no need of stirring. Methylene blue (MB) can be readily removed from aqueous solution by this Cu-BTC/ABS framework. The MB removal efficiency for solutions with concentrations of 10 and 5 mg/L was 93.3% and 98.3%, respectively, within 10 min. After MB adsorption, the Cu-BTC/ABS composite can easily be recovered without the need for centrifugation or filtration and the composite is reusable. In addition the ABS framework can be recovered for subsequent reuse. A significant advantage of 3D-printed frameworks is that different frameworks can be easily fabricated to meet the needs of different applications. This is a promising strategy to synthesize new frameworks using MOFs and polymers to develop materials for applications beyond adsorption.

The development of reactors, adsorbents and composites with unique structures has drawn great attention recently. These unique structures have advantages of improving reactivity, enhancing heat and mass transfer, lowering pressure drops and being easier to scale-up[1–10]. With the need for more sustainable and environmentally friendly production methods, the development and use of structured reactors will become even more important. Structured reactors are normally combined with porous materials like catalysts or adsorbents. In this regard, micro and meso inorganic porous materials have both been extensively applied.

Metal-organic frameworks (MOFs) are a new type of porous materials that are fabricated by linking metal ions or clusters and organic molecules (linkers) by strong bonds[11]. MOFs have ordered structures, permanent porosity, high surface area and can contain many different functional groups which make them useful for a variety of applications such as gas separation and storage, catalysis, energy storage, sensors, pollutant removal and biomedicine[12–21]. For example, Cu-BTC (also known as MOF-199, HKUST-1, or Cu_3BTC_2) reported for the first time by Chui *et al.*[22] was recently applied for gas storage and separation, catalysis and removal of pollutants[23–26] due to its large surface area, big pore volume, high Lewis acidity, good chemical stability, and ability of coordinated with water molecules. Recently, MOFs have been synthesized on various inorganic substrates, like alumina, silica, graphite oxide and ceramics[27–30].

MOFs are especially useful adsorbents for the removal of hazardous materials and there have been some reports of the use of MOFs in the adsorption of dyes[29,31]. The kinetics and thermodynamics of the adsorption of different dye materials by Cu-BTC/graphite oxide and MOF-235 have been investigated[29,31]. However, separating and recycling MOF adsorbents is complex, due to their brittleness and lack of flexibility. Organic materials like cellulosic fibrous, polysulfone, and polyvinylamine[32–34] have been used to prepare MOF polymer composites to improve performance in a variety of applications. Because of their ease of use, excellent stability at high pressures and resistance to acids and bases, polymers are good candidates for the fabrication of structured composites.

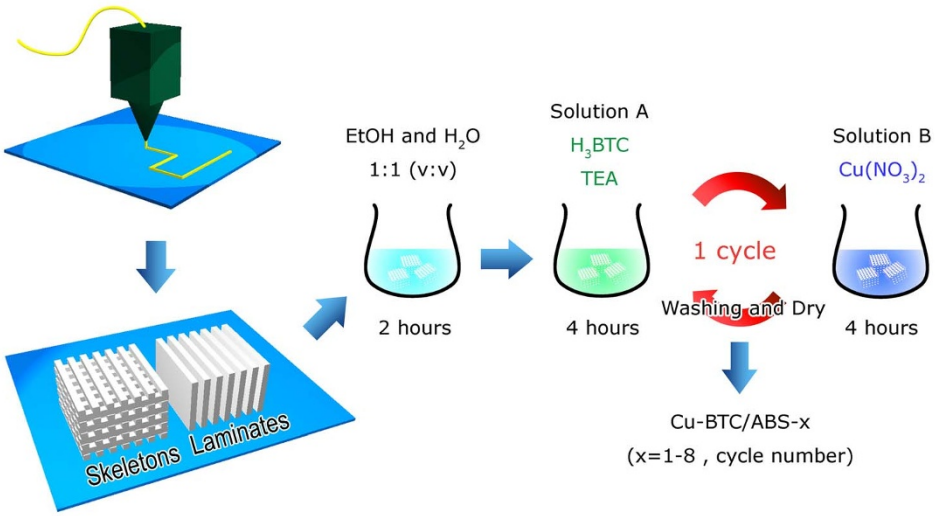

Figure 1 | Fabrication of Cu-BTC/ABS composites.

Herein, in order to enhance the flexibility of a MOF coated polymer composite, a three-dimensional (3D) printer was used to fabricate simple and complex acrylonitrile butadiene styrene (ABS) frameworks which were then coated with Cu-BTC. The Cu-BTC/ABS was then used as an absorbent to remove methylene blue from an aqueous solution. The recyclability and reusability of the Cu-BTC/ABS was also tested. To the best of our knowledge, this is the first report on the preparation of MOF composites by 3D printing. This is also the first 3D-printed materials used for dye adsorption.

Results

The overall synthetic procedure of Cu-BTC/ABS composite is schematically illustrated in Figure 1. The ABS framework was first printed using a 3D printer. Two kinds of frameworks were designed: (i) ABS polymer skeletons were printed for scanning electron microscopy (SEM), flame atomic absorption spectrometry (F-AAS) and the MB removal experiment; (ii) ABS polymer laminates were used for grazing incidence angle X-ray diffraction (GIAXRD), UV-vis spectroscopy and diffuse reflectance infrared Fourier transform (DRIFT) spectroscopy. Next, the printed ABS frameworks were cleaned by soaking in a 1 : 1 Ethanol (EtOH)/H_2O (v:v) solution for 2 h. The frameworks were then treated cyclically as follows: they were immersed in a solution of 1,3,5-benzenetricarboxylic acid (H_3BTC) and triethylamine (TEA) in 1 : 1 EtOH:H_2O for 4 h and then immersed in a solution of $Cu(NO_3)_2$ in 1 : 1 EtOH:H_2O for another 4 h and finally washed with 1 : 1 EtOH:H_2O and dried at room temperature (one cycle). After 1–8 cycles, turquoise Cu-BTC/ABS composites were obtained. Cu-BTC/ABS composites treated for 1–8 cycles were prepared and are labelled Cu-BTC/ABS-x, where x = 1–8 and represents the number of cycles. Pure Cu-BTC powders with no ABS were also synthesized under the same conditions and are labeled Cu-BTC.

Morphology and structure of the Cu-BTC/ABS composites. ABS skeletons were printed in the shapes of numbers and then each number-shape was subjected to that number of treatment cycles. The photographs of the Cu-BTC/ABS composites are shown in Figure 2. For the number 0 (pure ABS), the ABS skeleton is white. As the number of cycles increased, the color of the number-shaped ABS skeleton gradually changed from white to turquoise. In this regard, 3D-printed substrates have significant advantages over traditional injection molding methods since no molds are needed and sophisticated structures can be designed and fabricated.

Characterization of Cu-BTC/ABS composites. The pure ABS, pure Cu-BTC and Cu-BTC/ABS samples were further characterized by GIAXRD and the results are shown in Figure 3. The XRD patterns of pure Cu-BTC (Figure 3a) are in agreement with previously reported works[34,35], demonstrating that a pure Cu-BTC phase formed at room temperature in the water-ethanol solution. The XRD patterns of ABS contain a broad peak at ~19.7° and a shoulder at ~13.5° which are due to the amorphous structure of the copolymer (Figure 3b). The XRD patterns for the Cu-BTC/ABS samples resemble the ABS spectrum but there is also a new peak at peak at 11.6° (Figure 3c–f). At the number of cycles increased, this peak became stronger and sharper. The Cu-BTC/ABS-8 sample also has three other extra peaks (at 6.6°, 9.5° and 13.5°). These four peaks can be assigned to the (200), (220), (222) and (400) crystal planes of Cu-BTC, respectively. This proves that the turquoise coating on the surface of the ABS polymer is crystalline Cu-BTC.

This conclusion was further confirmed by UV-vis spectroscopy. As shown in Figure 4a, the spectrum of pure ABS contains no obvious peaks. However, for the Cu-BTC/ABS samples, a peak appears at 704 nm (Figure 4b–i) and as the number of cycles increased, the intensity of the peak gradually increased. This peak is due to the d-d band that is typical of Cu(II) carboxylate complexes[35] and has previously been reported[34,36]. These results indicate the formation of Cu-BTC on the ABS frameworks, corresponding with the XRD results.

Figure 5 shows the diffuse reflectance infrared spectra of the pure ABS and Cu-BTC/ABS samples at 1300–1700 cm^{-1}. For the pure

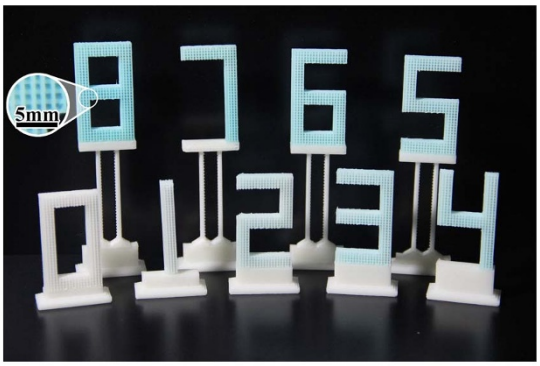

Figure 2 | Photographs of the synthesized Cu-BTC/ABS composites; the number represents the number of cycles (e.g. 1 = Cu-BTC/ABS-1).

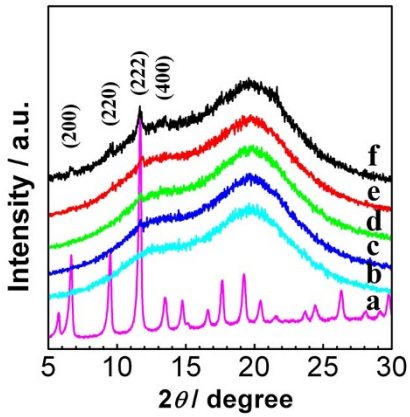

Figure 3 | XRD patterns of (a) pure Cu-BTC, (b) pure ABS, (c) Cu-BTC/ABS-2, (d) Cu-BTC/ABS-4, (e) Cu-BTC/ABS-6 and (f) Cu-BTC/ABS-8.

ABS, the weak bands at 1500 and 1460 cm^{-1} are attributed to the C–C vibrations of the mono-substituted aromatic ring. In the Cu-BTC/ABS samples, the peak at 1500 cm^{-1} gradually disappears and the peak at 1460 cm^{-1} shifts to 1450 cm^{-1}. This is probably the result of the mono-substituted aromatic rings on the surface of ABS being gradually covered by the tri-substituted aromatic rings of BTC. These results suggest that the ABS surface is coated with a high density of Cu-BTC and this was further investigated by SEM. The two very strong peaks at 1650 and 1376 cm^{-1} correspond to the asymmetric and symmetric vibrations of the deprotonated carboxylate (COO^-) groups of Cu-BTC respectively.

The morphologies of the pure ABS and the Cu-BTC/ABS composites prepared by the cyclic *in-situ* growth method were investigated by SEM. Figure 6a shows the SEM images of the ABS polymer skeleton. The surface of the printed ABS polymer skeleton is fairly smooth with some small hills which are due to the non-uniform heating and cooling that occurs during the 3D printing process. After the *in-situ* growth, Cu-BTC crystals are observed on the surface of the ABS (Figure 6b–e). For the 1st cycle, octahedral crystals with sizes ranged from 330 nm to 870 nm were homogeneously distributed on the surface of the ABS. The inset of Figure 6b shows a high resolution SEM image of a Cu-BTC crystal and in fact the crystal is not completely octahedral but is connected to the surface of the ABS skeleton. This suggests that the Cu-BTC particles grow directly on the ABS substrates.

After being treated for more cycles, more complex surface compositions were formed. The interactions between the polymer surface and the BTC linkers became non-uniform and therefore some smaller and biger Cu-BTC particles formed. So these samples had a wider particle size distribution and slightly smaller average particle sizes

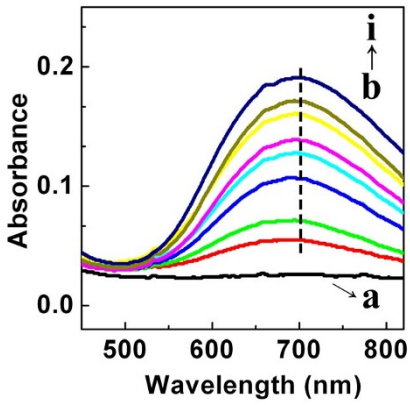

Figure 4 | UV-vis spectra of the Cu-BTC/ABS samples treated with different number of cycles. (a) pure ABS; (b)-(i) Cu-BTC/ABS-1 to 8.

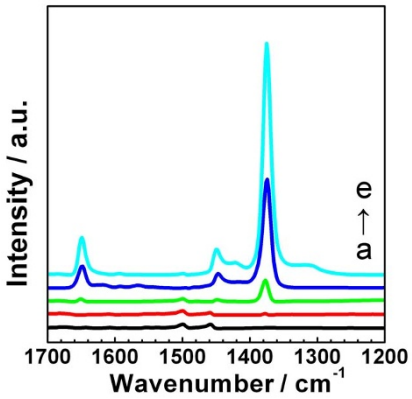

Figure 5 | Diffuse reflectance infrared spectra of the Cu-BTC/ABS samples treated with different number of cycles. (a) pure ABS; (b) Cu-BTC/ABS-2; (c) Cu-BTC/ABS-4; (d) Cu-BTC/ABS-6; and (e) Cu-BTC/ABS-8.

(Figure 6f and g). The Cu-BTC particle size in the Cu-BTC/ABS-8 sample was ranged from 200 nm to 900 nm. In addition, the formation of Cu-BTC improved the wettability of the surface which helps to adsorb more linkers and metal ions. This leads to a higher and thicker coverage of Cu-BTC. After the 8th cycle, the Cu-BTC/ABS-8 sample (Figure 6e) was almost completely covered with a thick layer of Cu-BTC which is in good agreement with the diffuse reflectance infrared spectra results.

Adsorption performance of Cu-BTC/ABS. The removal of MB from aqueous solution by the Cu-BTC/ABS composites was monitored by UV-vis spectroscopy. The amount of MB adsorbed and the MB removal efficiency are linearly increased with the loading amount of Cu-BTC. Here the Cu-BTC/ABS-8 composite was chosen as an illustration to show the capability of the Cu-BTC/ABS composite for MB adsorption. Figure 7 shows the adsorption performance of the Cu-BTC/ABS-8 composite towards 10 and 5 mg/L MB solutions. After 2 min of interaction with both MB solutions (Figure 7a and b), the intensity of the MB adsorption peak at 664 nm decreased significantly. When the adsorption time was extended to 10 min, the intensity decreased to a very low level. As shown in Figure 7c and d, the color change of the MB solution before and after adsorption confirms the UV-vis results. When the composite was directly removed by a hook from the MB solution, the liquid became clear and almost colorless, suggesting that it is easy to achieve a rapid separation and an efficient purification of water. Moreover, the blank experiment confirms that ABS has no adsorption capability. The hydrophobic ABS skeleton is even hard to be wetted by MB solution. The adsorption is only influenced by the loading of Cu-BTC.

The amounts of MB adsorbed per unit mass of Cu-BTC (q_t) and the MB removal efficiencies were calculated and are shown in Figure 7e and f. The maximum q_t values for Cu-BTC/ABS-8 were 64.3 and 33.9 mg/g for the 10 and 5 mg/L MB solutions respectively. The removal efficiencies for both MB solutions were high, even after only 10 min, and the removal efficiencies reached 93.3% and 98.3% for the 10 and 5 mg/L solutions respectively.

Regeneration of Cu-BTC/ABS and recycling of ABS. To evaluate the possibility of regenerating and reusing the Cu-BTC/ABS as an adsorbent, desorption experiments were performed. The used Cu-BTC/ABS-8 composite was repeatedly soaked in methanol to regenerate it and then it was reused to adsorb MB. The MB removal efficiencies of 1–5 cycles were calculated and are shown in Figure 8. The adsorption of MB in Cu-BTC includes both physical and chemical adsorption processes. Physical adsorption is the result

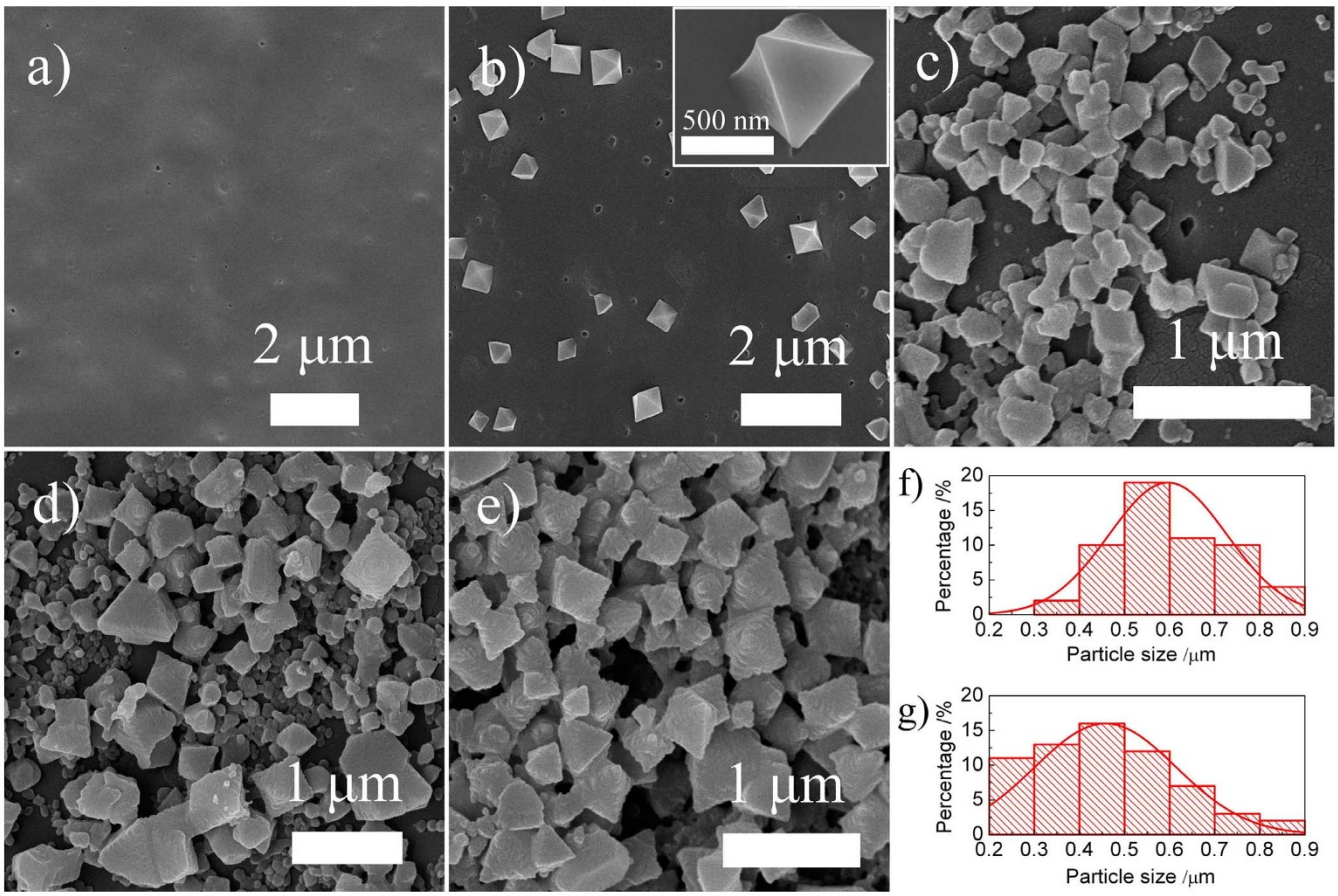

Figure 6 | SEM images of (a) pure ABS, (b) Cu-BTC/ABS-1, (c) Cu-BTC/ABS-3, (d) Cu-BTC/ABS-5 and (e) Cu-BTC/ABS-8; (f) and (g) particle size distributions of Cu-BTC/ABS-1 and Cu-BTC/ABS-8; inset of (b) is high resolution SEM image of Cu-BTC/ABS-1.

of capillary action in the Cu-BTC micropores and the MB is adsorbed as a neutral species. Chemical adsorption occurs when the MB nitrogen atoms coordinate with the copper atom in Cu-BTC and in this case MB is adsorbed as a charged ion. MB that adsorbs via physical adsorption can be eluted by an eluent, but chemically adsorbed MB cannot. Therefore, it has been shown in Figure 8 that when Cu-BTC/ABS is used two or more times, its removal efficiency greatly decreased. After reusing several times, the chemical adsorption sites become saturated, and physical adsorption becomes the main factor that contributes to adsorption. Li *et al.* used acetone as an eluent and proved that physical adsorption plays a major role in MB adsorption processes[29]. However, acetone causes ABS polymers to swell which will damage the 3D structure. So here methanol was chosen as the eluent. After five cycles, the MB removal efficiency was still over 58% (10 mg/L) and 68% (5 mg/L). These results show that the Cu-BTC/ABS-8 composite can be cyclically used.

The synthesis of the Cu-BTC/ABS composites uses large amounts of ABS. Therefore, the ability to recycle the ABS polymer is crucial for its practical applications. After five MB adsorption-desorption cycles, the dark-blue Cu-BTC/ABS-8 composites were immersed in 0.005 M HCl aqueous solution for 2 min and then removed. The immersion process was repeated five times. The photos of the recycling process are shown in Figure 9. After washing with aqueous HCl, the ABS polymer skeleton became white and could be used as a new substrate for secondary step-by-step growth. So this is a rapid and convenient method to recycle the used ABS polymer skeleton.

Discussion

Cu-BTC/ABS frameworks or composites were synthesized by combining 3D printing technology and step-by-step *in-situ* growth, and their performance for removing MB was investigated. Forming the ABS polymer skeleton by 3D printing has the advantages of flexible control of the structure and rapid manufacturing. The prepared Cu-BTC/ABS composites had a high coverage of Cu-BTC and exhibited considerable adsorption capacities and high removal efficiencies for MB from an aqueous solution. The Cu-BTC/ABS adsorbent can be easily separated from the MB solution with no need for centrifugation, filtration or magnetic separation. The Cu-BTC/ABS composites can be reused repeatedly and the ABS polymer skeleton can be recovered and reused for secondary Cu-BTC growth. This research shows that the Cu-BTC/ABS composite could potentially serve as an efficient adsorbent for environmental cleanup, and that 3D printing could be a rapid and eco-friendly method for preparing new functional composites for applications beyond adsorption.

Methods

3D Printing of ABS polymer. The 3D printing of ABS was performed using a HOFI-X1 3D Printer (Nanjing Baoyan Automation Co., Ltd. China). Filiform ABS polymer, as the printing raw material, was purchased from Nanjing Baoyan Automation Co., Ltd. The temperatures of the extruder and the 3D printer stage were set at 230 and 70°C, respectively. Two kinds of frameworks were designed: (i) ABS polymer skeletons were printed for scanning electron microscopy, flame atomic absorption spectrometry and the MB removal experiment; (ii) ABS polymer laminates were used for GIAXRD, UV-vis spectroscopy and DRIFT spectroscopy.

Synthesis of Cu-BTC/ABS composites. The Cu-BTC/ABS composites were prepared using a step-by-step *in-situ* growth method. Two solutions were prepared. Solution A consisted of 1,3,5-benzenetricarboxylic acid (0.6636 g, 3 mmol) and triethylamine (0.920 g, 9 mmol) dissolved in 60 mL of EtOH:H_2O (1 : 1 volume ratio). Solution B consisted of $Cu(NO_3)_2 \cdot 2.5H_2O$ (1.068 g, 4.5 mmol) dissolved in 60 mL of EtOH:H_2O (1 : 1 volume ratio). Next the printed ABS polymer skeleton (7.25 g) was immersed into 60 mL of 1 : 1 EtOH:H_2O for 2 h to clean and wet the surface. Then the preprocessed ABS polymer skeleton was treated with cyclic steps as follows: immersion in solution A for 4 h; immersion in solution B for 4 h; washing

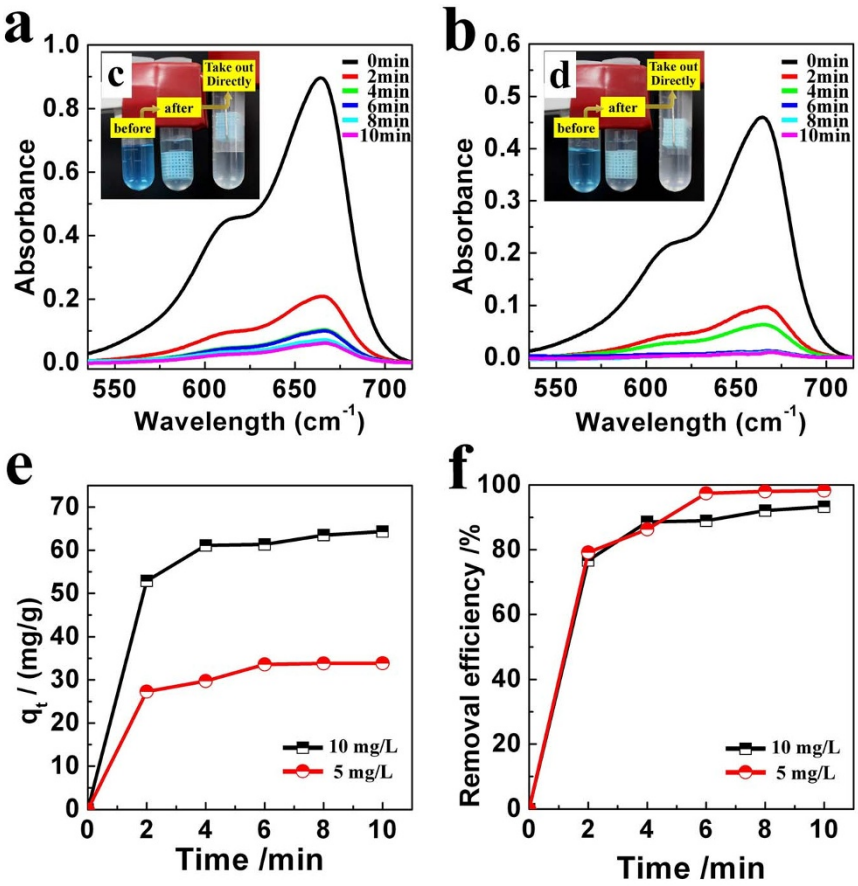

Figure 7 | (a-b) UV–vis spectra of 10 and 5 mg/L MB aqueous solutions during the adsorption in the presence of Cu-BTC/ABS-8; inset (c) and (d) photographs of 10 and 5 mg/L MB solutions during the adsorption; (e) the amount of MB adsorbed per unit mass; (f) the MB removal efficiency during the adsorption.

with 1 : 1 EtOH:H_2O and drying at room temperature (one cycle). After 1–8 cycles, turquoise Cu-BTC/ABS composites were synthesized. Pure Cu-BTC with no ABS was synthesized under similar condition: Solution A and B were mixed with stirring and reacted for 4 h. After filtering and drying, blue Cu-BTC powders were obtained.

Adsorption of methylene blue. The adsorption of MB on the Cu-BTC/ABS composites in aqueous solution was performed in a batch experiment. Typically, 145 mg of Cu-BTC/ABS-8 was added to 750 μL of MB aqueous solution with the desired initial concentration (10 or 5 mg/L). The mixture was shaken well for 2–10 min at room temperature. After adsorption, the Cu-BTC/ABS-8 composite was removed from the solution by using a hook. The adsorption of the MB molecules was monitored by UV-vis spectroscopy. The UV-vis spectra of MB were recorded from 520 to 730 nm and the MB concentration was quantified by measuring the adsorption intensity at 664 nm. The adsorption of MB on the pure ABS was also performed at same conditions, as blank experiment. The amount of MB adsorbed per unit mass of Cu-BTC and the removal efficiency of the MB were calculated according to the following equations:

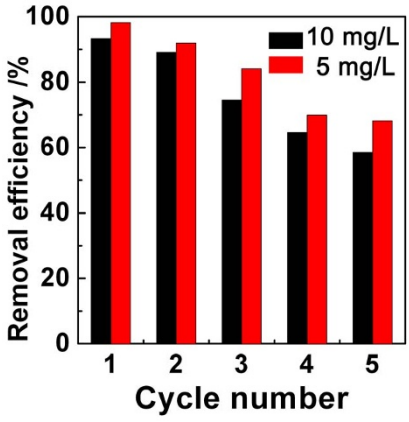

Figure 8 | **Removal efficiency over Cu-BTC/ABS-8 composite with increasing cycles.**

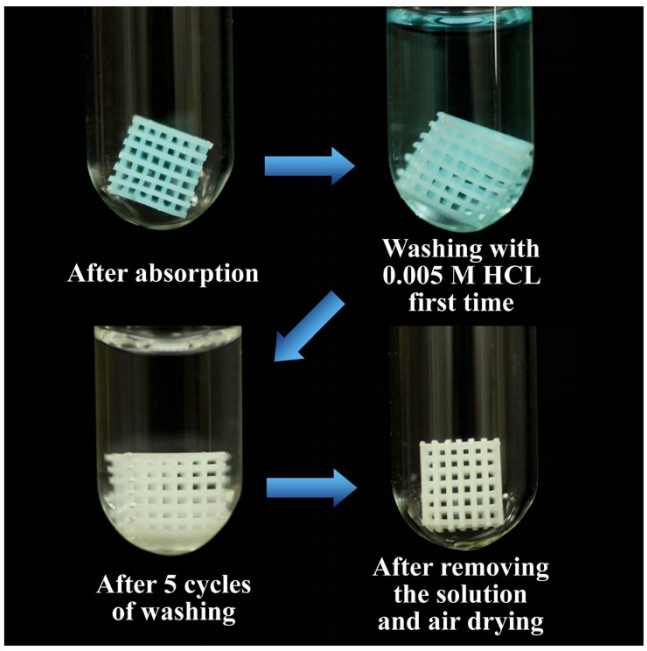

Figure 9 | **Photos of the recycling process of ABS polymer skeleton.**

$$q_t = \frac{(C_0 - C_e)}{m_{Cu-BTC}} \quad (1)$$

$$Removal\ efficiency\ \% = \frac{(C_0 - C_e)100}{C_0} \quad (2)$$

where q_t (mg/g) is the amount of MB adsorbed per gram of Cu-BTC; C_0 and C_e (mg/L) are the initial and residual concentrations of MB solution respectively; $m_{Cu\text{-}BTC}$ (g) is the mass of the Cu-BTC loaded on the adsorbent; and V (L) is the initial volume of the MB solution.

Regeneration of Cu-BTC/ABS composites and recycling of the ABS polymer skeleton. The feasibility for regenerating the Cu-BTC/ABS-8 composite after absorbing MB was evaluated using the solvent desorption technique. Methanol was used as the eluent to regenerate the Cu-BTC/ABS-8. The used Cu-BTC/ABS-8 samples were soaked in methanol and shaken for 6 h. The methanol was replaced with new methanol several times during the desorption process. The MB adsorption performance of the regenerated Cu-BTC/ABS-8 sample was then tested. The adsorption-desorption processes were repeated five times. After five adsorption-desorption cycles, the ABS polymer skeleton was recycled by immersing the exhausted Cu-BTC/ABS-8 into 0.005 M aqueous HCl for 2 min. The immersion process was repeated five times.

Characterization of Cu-BTC/ABS composites. The GIAXRD patterns of the samples were recorded on a Rigaku D/Max-2500 diffractometer at a scanning speed of 6°/min over the 2θ range of 5–30°. The diffractometer was equipped with a Ni-filtered Cu Kα radiation source (λ = 1.54056 Å). The morphology of the samples was characterized using SEM (FEI Nanosem430). SEM observation was conducted after pasting a piece of samples on conductive tape and coating a thin layer of gold by using a K575XD ion sputter (QUORUM, UK). UV-vis absorption spectra of the samples were recorded on a Beckman DU-8B UV–Vis spectrophotometer. DRIFT spectra were obtained on a Thermo Nicolet's Nexus 870 system at room temperature and in air. The DRIFT spectra were recorded with 32 scans and at a resolution of 4 cm^{-1}.

The compositions of the Cu-BTC/ABS composites were determined by immersing a weighed amount of Cu-BTC/ABS into 10 mL of 0.005 M HCl aqueous solution for more than 4 h. Then the sample was dissolved in aqueous HCl and the Cu concentration was determined using atomic absorption spectroscopy (Rayleigh Analytical Instrument Corp., China; WFX-130). The Cu-BTC content in the Cu-BTC/ABS composite was calculated according to the following equation:

$$Cu_3(BTC)_2\ wt\ \% = \frac{\boldsymbol{C \cdot V_0}}{\boldsymbol{m_0}} \times \frac{\boldsymbol{M[Cu_3(BTC)_2]}}{\boldsymbol{M[Cu]}} \quad (3)$$

Where C is the Cu concentration measured by AAS; V_0 is the volume of aqueous HCl; m_0 is the mass of the Cu-BTC/ABS composite; and $M[Cu_3(BTC)_2]$ and $M[Cu]$ are the molecular weight of $Cu_3(BTC)_2$ and Cu, respectively. The Cu-BTC/ABS-8 sample contained a total loading of 0.15 wt% Cu-BTC as measured by flame atomic absorption spectrometry.

1. Fan, X. L., Lapkin, A. A. & Plucinski, P. K. Liquid phase hydrogenation in a structured multichannel reactor. *Catal. Today* **147**, S313–S318 (2009).
2. Barth, K. A. *et al.* An Engineered Mannoside Presenting Platform: Escherichia coli Adhesion under Static and Dynamic Conditions. *Adv. Funct. Mater.* **18**, 1459–1469 (2008).
3. Kolb, G. & Hessel, V. Micro-structured reactors for gas phase reactions. *Chem. Eng. J.* **98**, 1–38 (2004).
4. Gensel, J. *et al.* Cavitation engineered 3D sponge networks and their application in active surface construction. *Adv. Mater.* **24**, 985–989 (2012).
5. Wang, H., Sun, K., Tao, F., Stacchiola, D. J. & Hu, Y. H. 3D honeycomb-like structured graphene and its high efficiency as a counter-electrode catalyst for dye-sensitized solar cells. *Angew. Chem. Int. Ed.* **52**, 9210–9214 (2013).
6. Pangarkar, K. *et al.* Structured packings for multiphase catalytic reactors. *Ind. Eng. Chem. Res.* **47**, 3720–3751 (2008).
7. Zheng, S. J., Carpenter, J. S., McCabe, R. J., Beyerlein, I. J. & Mara, N. A. Engineering interface structures and thermal stabilities via SPD processing in bulk nanostructured metals. *Sci. Rep.* **4**, 4226–4231 (2014).
8. Brandt, K., Wolff, M. F., Salikov, V., Heinrich, S. & Schneider, G. A. A novel method for a multi-level hierarchical composite with brick-and-mortar structure. *Sci Rep* **3**, 2322–2329 (2013).
9. Kang, W. S., Lee, D. H., Lee, J. O., Hur, M. & Song, Y. H. Combination of plasma with a honeycomb-structured catalyst for automobile exhaust treatment. *Environ. Sci. Technol.* **47**, 11358–11362 (2013).
10. Yu, L., Zhang, Y., Zhang, B. & Liu, J. Enhanced antibacterial activity of silver nanoparticles/halloysite nanotubes/graphene nanocomposites with sandwich-like structure. *Sci. Rep.* **4**, 4551–4555 (2014).
11. Eddaoudi, M. *et al.* Systematic design of pore size and functionality in isoreticular MOFs and their application in methane storage. *Science* **295**, 469–472 (2002).
12. Kwon, H. T. & Jeong, H. K. In situ synthesis of thin zeolitic-imidazolate framework ZIF-8 membranes exhibiting exceptionally high propylene/propane separation. *J. Am. Chem. Soc.* **135**, 10763–10768 (2013).
13. Jiang, H. L., Akita, T., Ishida, T., Haruta, M. & Xu, Q. Synergistic catalysis of Au@Ag core-shell nanoparticles stabilized on metal-organic framework. *J. Am. Chem. Soc.* **133**, 1304–1306 (2011).
14. Zhou, Y., Xiang, Z., Cao, D. & Liu, C. J. Preparation and Characterization of Covalent Organic Polymer Supported Palladium Catalysts for Oxidation of CO and Benzyl Alcohol. *Ind. Eng. Chem. Res.* **53**, 1359–1367 (2014).
15. Zhang, W. *et al.* Controlled incorporation of nanoparticles in metal-organic framework hybrid thin films. *Chem. Commun.* **50**, 4296–4298 (2014).
16. Xia, W. *et al.* Facile preparation of hierarchically porous carbons from metal-organic gels and their application in energy storage. *Sci. Rep.* **3**, 1935 (2013).
17. Li, W. J. *et al.* In situ growth of metal-organic framework thin films with gas sensing and molecule storage properties. *Langmuir* **29**, 8657–8664 (2013).
18. Yadav, M. & Xu, Q. Catalytic chromium reduction using formic acid and metal nanoparticles immobilized in a metal-organic framework. *Chem. Commun.* **49**, 3327–3329 (2013).
19. Lee, J. Y., Tang, C. Y. Y. & Huo, F. W. Fabrication of Porous Matrix Membrane (PMM) Using Metal-Organic Framework as Green Template for Water Treatment. *Sci. Rep.* **4**, 3740 (2014).
20. Della, R. J., Liu, D. & Lin, W. Nanoscale Metal-Organic Frameworks for Biomedical Imaging and Drug Delivery. *Accounts Chem. Res.* **44**, 957–968 (2011).
21. Sun, C. Y. *et al.* Chiral nanoporous metal-organic frameworks with high porosity as materials for drug delivery. *Adv. Mater.* **23**, 5629–5632 (2011).
22. Chui, S. S. Y., Lo, S. M. F., Charmant, J. P. H., Orpen, A. G. & Williams, L. D. A Chemically Functionalizable Nanoporous Material $[Cu_3(TMA)_2(H_2O)_3]_n$. *Science* **283**, 1148–1150 (1999).
23. Peng, Y. *et al.* Methane storage in metal-organic frameworks: current records, surprise findings, and challenges. *J. Am. Chem. Soc.* **135**, 11887–11894 (2013).
24. Shah, M. N., Gonzalez, M. A., McCarthy, M. C. & Jeong, H. K. An unconventional rapid synthesis of high performance metal-organic framework membranes. *Langmuir* **29**, 7896–7902 (2013).
25. Ye, J. Y. & Liu, C. J. $Cu_3(BTC)_2$: CO oxidation over MOF based catalysts. *Chem. Commun.* **47**, 2167–2169 (2011).
26. Ke, F. *et al.* Thiol-functionalization of metal-organic framework by a facile coordination-based postsynthetic strategy and enhanced removal of Hg2+ from water. *J. Hazard. Mater.* **196**, 36–43 (2011).
27. Mao, Y. Y., Cao, W., Li, J. W., Sun, L. W. & Peng, X. S. HKUST-1 Membranes Anchored on Porous Substrate by Hetero MIL-110 Nanorod Array Seeds. *Chem. Eur. J.* **29**, 11883–11886 (2013).
28. Sachse, A. *et al.* In situ synthesis of Cu-BTC (HKUST-1) in macro-/mesoporous silica monoliths for continuous flow catalysis. *Chem. Commun.* **48**, 4749–4751 (2012).
29. Li, L. *et al.* A MOF/graphite oxide hybrid (MOF: HKUST-1) material for the adsorption of methylene blue from aqueous solution. *J. Mater. Chem. A* **1**, 10292–10299 (2013).
30. Granato, T., Testa, F. & Olivo, R. Catalytic activity of HKUST-1 coated on ceramic foam. *Microporous Mesoporous Mater.* **153**, 236–246 (2012).
31. Haque, E., Jun, J. W. & Jhung, S. H. Adsorptive removal of methyl orange and methylene blue from aqueous solution with a metal-organic framework material, iron terephthalate (MOF-235). *J. Hazard. Mater.* **185**, 507–511 (2011).
32. Silva Pinto, M., Sierra-Avila, C. A. & Hinestroza, J. P. In situ synthesis of a Cu-BTC metal–organic framework (MOF 199) onto cellulosic fibrous substrates: cotton. *Cellulose* **19**, 1771–1779 (2012).
33. Nagaraju, D., Bhagat, D. G., Banerjee, R. & Kharul, U. K. In situ growth of metal-organic frameworks on a porous ultrafiltration membrane for gas separation. *J. Mater. Chem. A* **1**, 8828–8835 (2013).
34. Meilikhov, M. *et al.* Stepwise deposition of metal organic frameworks on flexible synthetic polymer surfaces. *Dalton Trans.* **40**, 4838–4841 (2011).
35. Mao, Y. Y. *et al.* Room temperature synthesis of free-standing HKUST-1 membranes from copper hydroxide nanostrands for gas separation. *Chem. Commun.* **49**, 5666–5668 (2013).
36. Nan, J. P., Dong, X. L., Wang, W. J., Jin, W. Q. & Xu, N. P. Step-by-step seeding procedure for preparing HKUST-1 membrane on porous alpha-alumina support. *Langmuir* **27**, 4309–4312 (2011).

Acknowledgments

This work was supported by the National Natural Science Foundation of China (#91334206). The authors thank Dr. Jeanne Wynn for her help in the use of English.

Author contributions

Experiments were designed by C.J.L. and Z.Y.W. and performed by Z.Y.W., J.J.W., M.Y.L. and K.H.S. Results were analyzed and interpreted by Z.Y.W., J.J.W., M.Y.L. and K.H.S. The manuscript was written by Z.Y.W. and C.J.L. C.J.L. is in charge of the project direction, planning and organization.

Additional information

Competing financial interests: The authors declare no competing financial interests.

How to cite this article: Wang, Z.Y., Wang, J.J., Li, M.Y., Sun, K.H. & Liu, C.-J. Three-dimensional Printed Acrylonitrile Butadiene Styrene Framework Coated with Cu-BTC Metal-organic Frameworks for the Removal of Methylene Blue. *Sci. Rep.* **4**, 5939; DOI:10.1038/srep05939 (2014).